8th International Conference

on

Wind Turbine Noise

Lisbon – 12th to 14th June 2019

Hydrodynamic Analysis of Trailing Edge Serrations with Blunt and Rounded Edges

Alper Celik, Bin Zang, Yannick D. Mayer, Xiao Liu and Mahdi Azarpeyvand*
University of Bristol, Bristol, United Kingdom, BS8 1TR

Summary

A comprehensive experimental study is performed to examine the effects of large serrations on the surface pressure fluctuations of a flat plate test rig. Two different configurations, consisting of a sharp edge profile and a rounded edge profile, are tested to understand the effect of serrations on the noise generated at the trailing edge and the associated flow field, compared to a straight trailing edge flat plate. The test rig is heavily instrumented with microphones and pressure taps. The tests are performed at serration root-to-tip distance based Reynolds number of $Re = 1.8x10^5$. The results are presented for a range of frequencies $50Hz < f < 6000Hz$, where a broadband noise increase is observed around $f \simeq 150 - 200Hz$ for both serrated configurations. It is shown that the structures generating the increase in the energy content in low frequencies evolve through the leading edge, then gain strength as they develop downstream and amalgamate at the tip of the serration. This was confirmed by both the sound pressure level results and the surface pressure coherence analysis.

*Corresponding Author, m.azarpeyvand@bristol.ac.uk

1. Introduction

Over the last few decades, the increased air traffic and rapidly developing wind turbine farms in urban and rural areas accelerated the concerns about noise emissions. Aerodynamic noise generated by the turbulent flow past a trailing edge over the airfoil is one of the most important sources of noise. Among all the mechanisms that Brooks *et al.* [1] have shown to contribute to airfoil self-noise, turbulent boundary layer interaction with the trailing edge is the main source generating the broadband noise. The increased awareness about noise pollution and foreseen noise pollution reduction targets by institutions (such as ACARE Flightpath 2050), researchers have focused on decreasing the noise levels of these inseparable instruments of modern life. Several passive control methods including brushes [2], leading and trailing edge serrations [3, 4, 5, 6] as well as the active control techniques such as wall-normal suction [7, 8] and blowing [9] or dielectric barrier discharge plasma actuators [10] have been investigated in the literature. Serrations, geometry which is inspired by the wing of an owl, is the most common method applied owing to its easy application and relatively low effects on the aerodynamic performances [11].

Analytical models initiated by Howe [12] to predict the noise reduction by the serrated trailing edges over predicts the noise reduction level. Although the models keep evolving with new studies such as Lyu *et al.* [3, 13, 14],the integration to calculate the far-field noise from wall pressure fluctuations requires the assumption of frozen turbulence. With this assumption the statistical properties of the convected eddies over the trailing edge is assumed to be not effected by the existence of the trailing edge which leads the pressure spectra to be formulated at the trailing edge in cartesian coordinate based wave numbers. These pressure spectra are then propagated to calculate far-field noise. Recent studies show that these assumptions might be considered to be the main source of error in predicted noise levels [15]. Having a non-straight trailing edge, the boundary layer and associated pressure spectra change through the leading edge of the serration. These changes in the pressure spectra on the serration should be taken into account to improve far-field noise predictions.

The necessity to obtain a sound knowledge on the flow structures and pressure spectra on the serration geometry accelerated both numerical [16, 17, 18] and experimental studies [2, 19, 20, 21]. In their DNS study [16], Jones and Sandberg showed that a highly three-dimensional flow dominates the tip of the serration, where stream-wise vortices from upstream smoothly develop into span-wise vortices. Recently conducted experimental studies [15, 20, 22, 21], support the outcomes of the numerical studies. However, there lacks a common view on how the serrations mitigate the broadband noise.

This investigation aims to map the wall pressure fluctuations and corresponding spectra in detail over a serration geometry. To achieve a highly instrumented serration geometry considering the size restrictions due to microphones, a set of relatively large serrations were manufactured. The serration root-to-tip length is five times the boundary layer height developed on the serration. Although the design may not appear to be optimal, the authors believe that most of the results are applicable to serrations of normal dimensions. The results may also shed light on serrated airfoils or wind turbine blades operating in sub-optimal conditions.

2. Experimental Set-Up

The experiments were performed in the University of Bristol Aeroacoustic Facility, which is a closed-circuit, open-jet anechoic wind tunnel. The anechoic chamber has a cut-off frequency of 160Hz with physical dimensions of 6.7m x 4.0m x 3.3m and the nozzle has an area of 500mm x 775mm which allows a steady operation from 5m/s to 45m/s. The experiments were performed for a range of flow velocities $10m/s \leq U_\infty \leq 40m/s$ with turbulence intensity levels below 0.2% [23]. For brevity, only the results at free stream velocity of $30m/s$ is presented.

To understand the flow physics over serrations, a highly instrumented flat plate test-rig was designed and manufactured at the University of Bristol. A total number of 84 Knowles FG-23329-P07 miniature pressure transducers were instrumented to obtain a very detailed near-field pressure map and allow possible future experiments the flat plate test. 75 microphones were installed on the serrations and 8 were installed on the flat plate. The microphones are 2.6mm in diameter with a circular sensing area of 0.8mm. The serrations and flat plate were machined to have 0.4mm pinhole mask to avoid pressure attenuation at high frequencies.

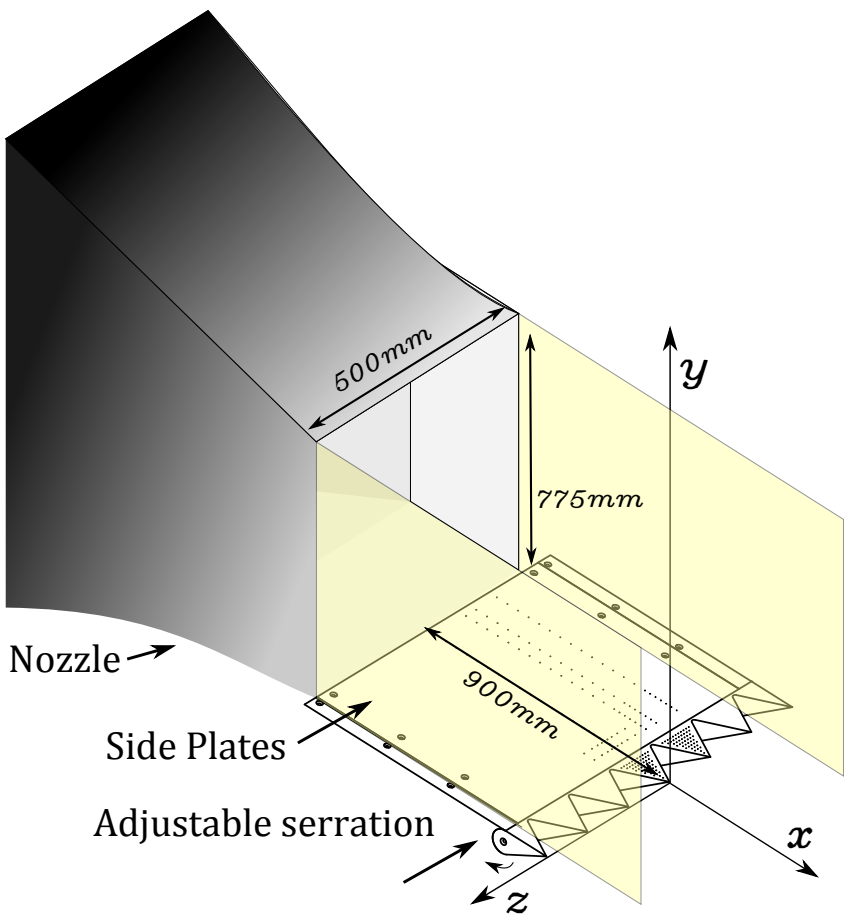

Figure 1 Schematics of the flat plate serration rig.

Velocity measurements were conducted using a 55P16 single-wire constant temperature hot-wire anemometry (CTA). Dantec StreamlinePro CTA 91C10 modules were used with 55P16 single-wire

probes. The probes was calibrated by using the Dantec 54H10 type calibrator. The probe was controlled with a two-axis ThorLabs LTS300M traverse system.

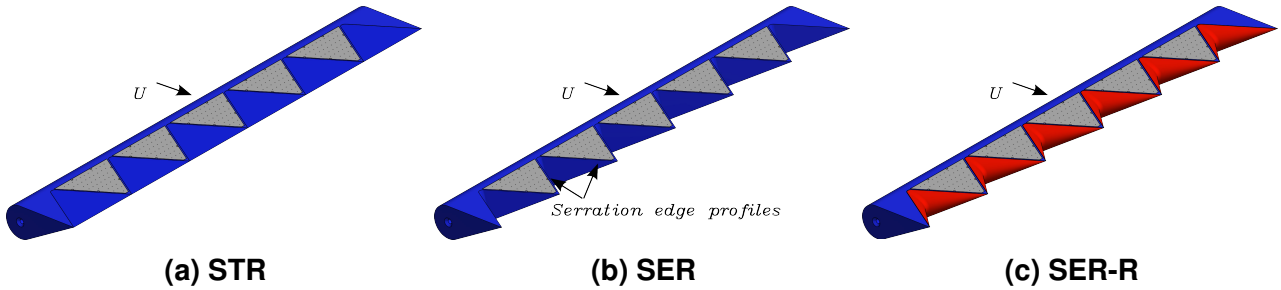

Figure 2 Schematics of the trailing edge models a) Straight trailing edge (STR) b)Serrated trailing edge (SER) and c) Serrated and rounded trailing edge (SER-R)

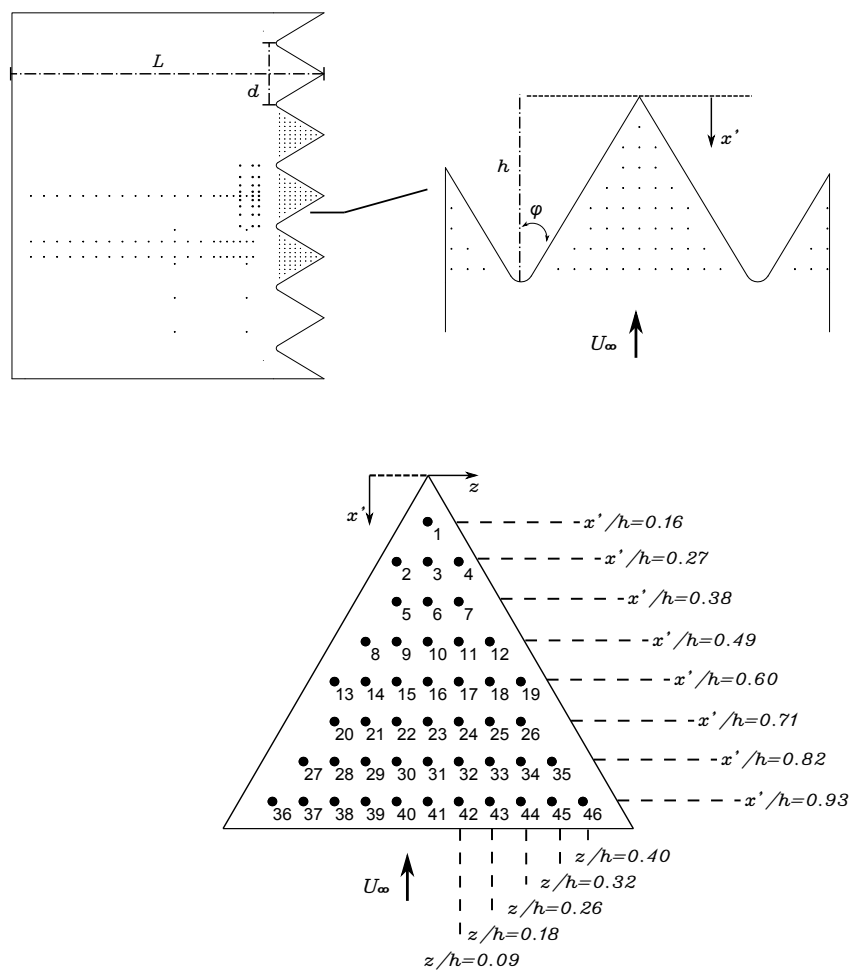

Figure 3 Schematics and geometric details of the flat plate model.

All near-field and hot-wire measurements were performed for 16 seconds at a sampling frequency of $2^{16}Hz$. The near-field and hot-wire data were acquired by using four National Instrument PXI-e4499

cards and were driven by a Matlab script. Pressure measurements were carried out using two 32 channel Chell MicroDAQ pressure scanners at a sampling frequency of 1000Hz for 16 seconds. The scanners have a full-scale accuracy of 0.05%. The averaged results were used to present non-dimensional pressure coefficient C_{prms}.

Figure 1 illustrates the flat plate rig mounted to the lower lip of the wind tunnel nozzle. Side plates were used to assure the two-dimensionality of the flow. The serration part can be tilted around z-axis to have an angle with respect to free stream flow. The serration can be adjusted for different angles from 0° to 30°. 3-D printed add-on fillings were used to obtain a straight trailing edge and rounded trailing edge. Schematics of these fillings are demonstrated in Figure 2. The experiments were conducted for the free-stream velocity of $U = 30m/s$, which corresponds to serration chord based Reynolds number of $Re \approx 1.8x10^5$.

The geometric details of the flat-plate rig are presented in Figure 3. The total length of the rig was $L = 0.9m$. Serration root-to-tip distance is $h = 0.091m$ and span-wise width is $d = 0.105m$. The serration angle is $\varphi = 32°$. A local coordinate x' is designated to clarify the microphone locations, as shown in Figure 3. The stream-wise and span-wise locations are labeled and presented at the bottom row of Figure 3. Taps used for the steady pressure measurements had the same spatial distribution as microphone locations.

3. Results & Discussion

3.1. Surface pressure fluctuations over the serration

The power spectral density (PSD) of the pressure fluctuations measured at each microphone is calculated as

$$\phi_{pp}(dB/Hz) = 20\log_{10}\left(\frac{\overline{p}'}{\overline{p}_{ref}}\right), \tag{1}$$

where $\bar{p}'$ refers to the averaged pressure fluctuations and $p_{ref} = 20\mu Pa$ is the reference pressure. $\bar{p}'$ was obtained by converting the power spectral density of the measured signal at each microphone to pressure. Figure 4 demonstrates the comparison of the ϕ_{pp} values for the straight trailing edge (STR), serrated trailing edge (SER), and the combined serrated and rounded trailing edge (SER-R) cases for microphone 1 at the tip of the serration ($x'/h = 0.16$). The ϕ_{pp} results for the STR demonstrate a 6dB linear decay from 100Hz to 1000Hz, which could be interpreted as a sign of an attached turbulent boundary layer flow. The serrated trailing edge results demonstrate a completely different phenomenon with a broadband ϕ_{pp} hump between $50Hz < f < 600Hz$, which implies an increase in the energy content at low frequencies. SER-R results have a similar trend to that of SER. However, the broadband hump has a lower peak magnitude and elongates towards lower frequencies. These broadband humps may be the footprint of a large scale hydrodynamic field and will be investigated in the following sections.

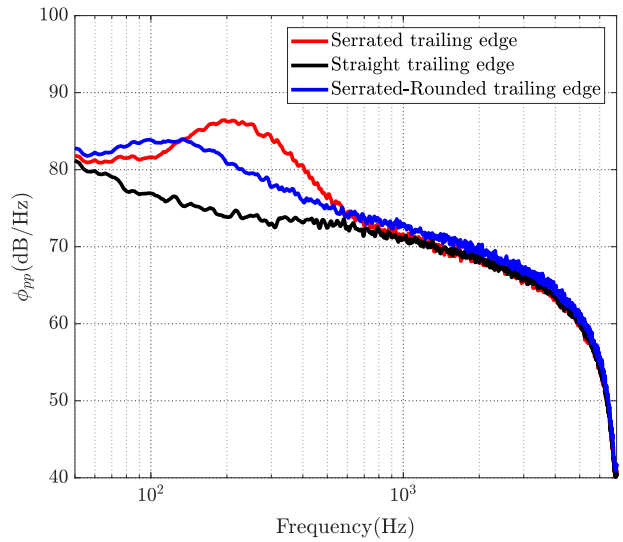

Figure 4 Comparison of the power spectral density of the pressure fluctuations for Straight trailing edge (STR), Serrated trailing edge (SER), and Serrated and rounded trailing edge (SER-R) at microphone location 1, $x'/h = 0.16$**,** $p_{ref} = 20\mu Pa$

Figure 5 further investigates the source of the energy content increase, where the ϕ_{pp} graphs for microphones at locations 3,6,10,16 (stream-wise), and 4,7,12,19 (along the edge profile) are shown on the left and right column of the figure, respectively. In the case of the STR trailing-edge, a similar trend is observed for all the measurement locations, as expected. The SER case, however, shows a distinct characteristic when all the figures are examined. Along the serration mid-plane on left hand side column, the broadband hump does not appear until the tip of the serration. On the contrary, following the edge of the serration, the broadband hump exists even at microphone location 19, and gradually increases in magnitude towards the tip for the SER case. This may be interpreted as the footprint of the physical structures evolving on the serration edge profile (on both sides) and amalgamating at the tip, which was also discussed in [21]. For the SER-R case, where the sharp edge profile was changed with rounded edge profiles, the broadband hump exists at a lower frequency range, peaked at around $f = 150Hz$. Moreover, the magnitude of the peak is lower compared to SER case above $\approx 200Hz$, but higher below that.

Contours of non-dimensional root-mean-square (RMS) coefficients for the pressure fluctuations p' are presented in Figure 6. The $C_{p_{rms}}$ values were calculated using Equation 2, where p_i is the ith data measured, $\bar{p'}$ refers to the averaged pressure over the entire measurement duration, and the dynamic pressure p_{dyn} was calculated based on free stream velocity. The very dense contours at the edges are due to interpolation between the zero valued cells and the measured region, hence should not be taken into consideration.

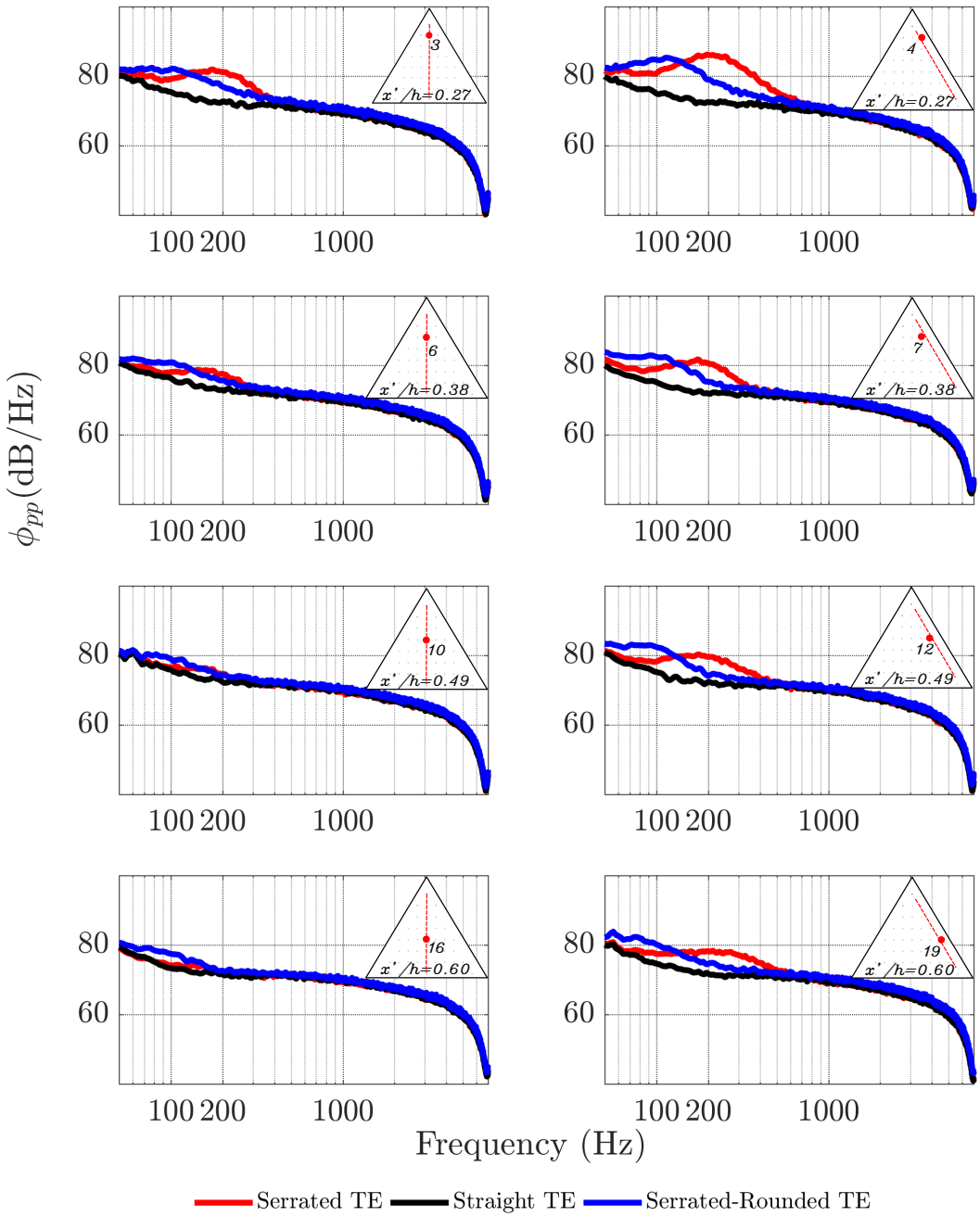

Figure 5 Comparison of the power spectral density of the pressure fluctuations measured at microphones 3,6,9,16 (stream-wise, on left column) and 4,7,12,19 (leading-edge, on right column) for STR, SER and SER-R, $p_{ref} = 20\mu Pa$

$$C_{p_{rms}} = \frac{\sqrt{\sum_{i=1}^{N}(p_i - \bar{p})^2/N}}{p_{dyn}}, \tag{2}$$

Considering the STR case, $C_{p_{rms}}$ value is mostly evenly distributed with a slight increase towards the trailing edge. For both the SER and SER-R cases the $C_{p_{rms}}$ values increase significantly compared to the STR case. For the SER case specifically, the increase is more pronounced at the tip, and the footprint of the leading edge structures can be seen on the left edge with very high $C_{p_{rms}}$ values. At $x'/h = 0.93$, where the connection with flat plate starts, a low $C_{p_{rms}}$ region is observed. The results of the SER-R are very similar to that of the SER, where the increased $C_{p_{rms}}$ region is more symmetrical with respect to the symmetry plane of the serration.

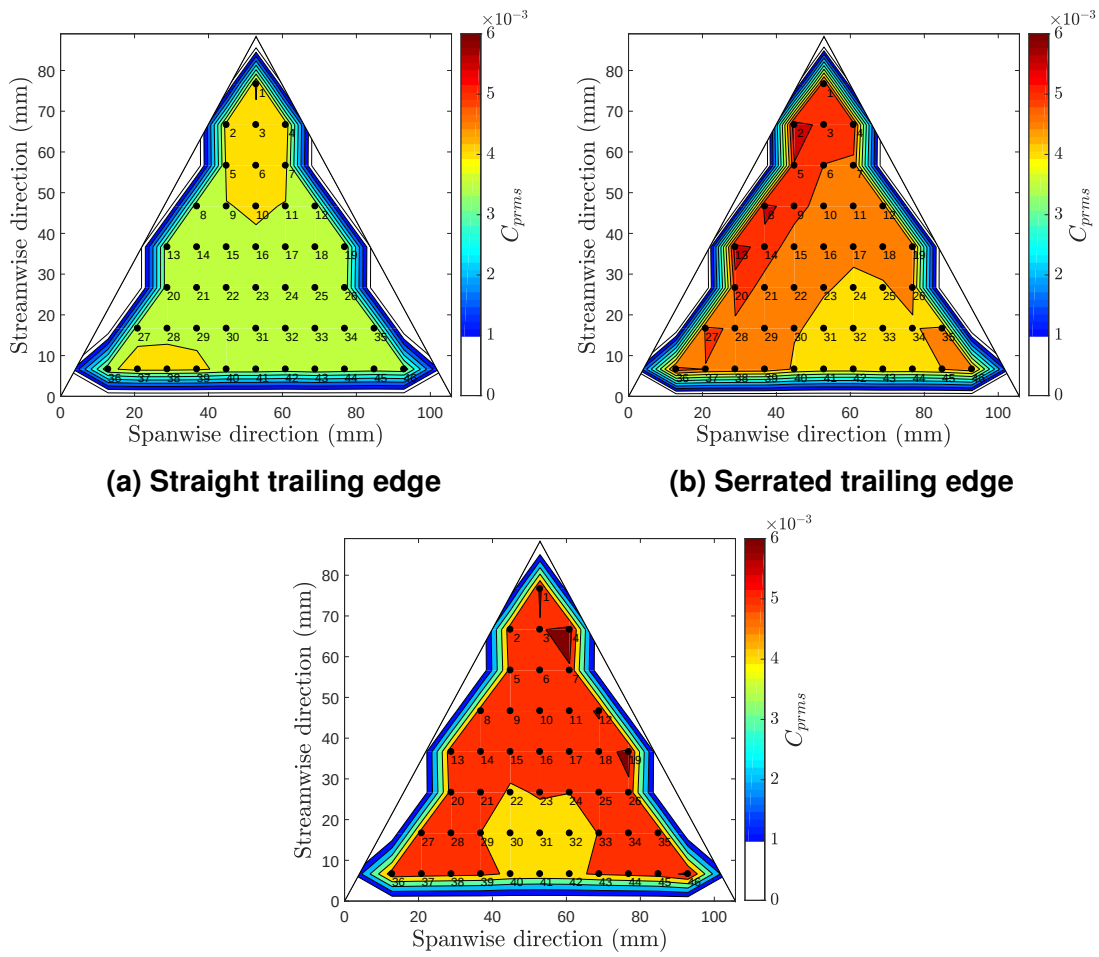

(a) Straight trailing edge

(b) Serrated trailing edge

(c) Serrated and rounded trailing edge

Figure 6 Contours of non-dimensional pressure fluctuations C_{prms} for STR, SER and SER-R cases.

3.2. Surface pressure correlation analysis

3.2.1. Span-wise coherence and length scale

The span-wise coherence and the associated length scales are widely used tools to study the coherent structures in the flow. As briefly discussed in the introduction, the span-wise length scale of the structures have a crucial role in the prediction of the far-field noise from wall pressure fluctuations. The magnitude-squared span-wise coherence and associated length scales can be calculated from

$$\gamma^2_{p'_i p'_j} = \frac{\left|\phi_{p'_i p'_j}\right|^2}{\left|\phi_{p'_i p'_i}\right|\left|\phi_{p'_j p'_j}\right|}, \tag{3}$$

and

$$\Lambda_p = \int_0^\infty \gamma_{p'_i p'_j}\left(\xi_z\right) d\xi_z, \tag{4}$$

where $\gamma^2_{p'_i p'_j}$ stands for the span-wise coherence calculated between two microphones as i and j. $\phi_{p'_i p'_j}$ stands for the cross-power spectral density, and ξ_z represents the span-wise distance between two microphones.

Figure 7 presents the span-wise coherence results at five different stream-wise locations $x'/h = 0.16, 0.27, 0.38, 0.49, 0.6$ and $x'/h = 0.93$. The very left column represents serration and shows the microphones used to calculate the span-wise coherence. In Figure 7, the marker "x" stands for the reference microphone. The microphones, which were used to calculate the coherence with respect to the reference microphone, are colour-coded. The same colour-code is also implemented in the graphs to ease the interpretation. The rest of the columns from left to right represent the STR, SER and SER-R configurations.

Considering the results of the straight trailing edge case, i.e., STR, the span-wise coherence between the reference microphone and the closest microphones (mic3-4,mic6-7,mic10-11 and mic16-17) does not change significantly for all the locations examined. The broadband hump between $100Hz < f < 1000Hz$ peaks at $f = 400Hz$. The magnitude of the coherence decreases towards upstream locations,i.e, $x'/h = 0.93$. However, for the serrated case, the magnitude of the span-wise coherence at $x'/h = 0.27$ between microphones 3 and 4 significantly increases compared to the STR case, which may an indication of an increase in length scale of the structures. The peak frequency for the span-wise coherence occurs at $200Hz$, which coincides with the peak observed in ϕ_{pp} graphs for the SER. The use of the rounded serration edge profiles decrease the magnitude of the coherence, which means the structures created by this case are smaller compared to the SER.

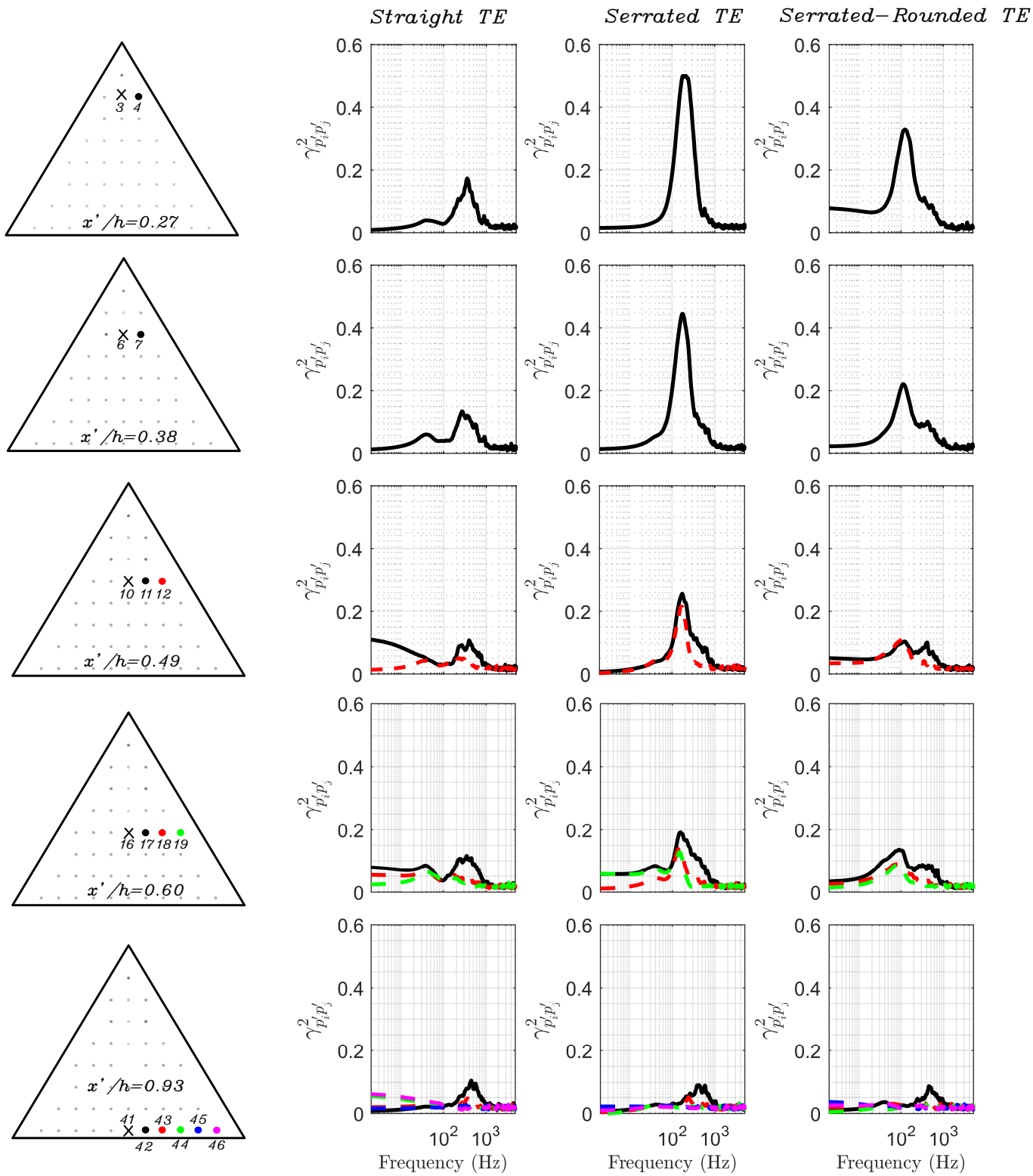

Figure 7 Comparison of span-wise $\gamma^2_{p'_i p'_j}$ among the STR, SER and SER-R at stream-wise stations $x'/h = 0.27, 0.38, 0.49, 0.60$ and $x'/h = 0.93$ from top to bottom.

Comparing all the coherence results over the entire serration, from $x'/h = 0.27$ to upstream $x'/h = 0.83$, from bottom row to top row, the use of STR is observed to cause a very slight increase in coherence values. Although all three cases have the same coherence behaviour at the very upstream station $x'/h = 0.93$, the SER and SER-R gradually increase their coherence value with the closest microphones at each station. This observation is in good agreement with those reported [20]. The results clearly show that trailing edge serrations have a significant effect on the span-wise coherence of the flow structures, and the intensity of the effect varies depending on the edge profile.

Figure 8 displays the effect of serration on the length scales of the coherent structures and the evolution of these structures from the root of the serration to the tip along the serration edge profile. The calculations were performed at $x'/h = 0.60$, among microphones 16,17,18 and 19 using Equation4. The figure shows that at high frequencies ($f > 1000Hz$) all three configurations converge, mostly due to limited spatial resolution. At lower frequencies, the three cases exhibit unique behaviour. The SER case has a peak at around $f = 160Hz$, which was previously observed in ϕ_{pp} and span-wise coherence results at $x'/h = 0.60$. The magnitude of the length scale nearly doubles the magnitude of straight trailing edge. Similarly the SER-R also exhibits a peak at around $f = 100Hz$ with a 50% magnitude increase compared to STR case. Moreover, this result supports the idea of relatively stronger turbulence activities occur on the trailing edge when it is serrated, compared to a straight one. Hence, far-field predictions based on the frozen turbulence assumption, which assumes there is no change in turbulence behaviour on the trailing edge, should consider length scale changes observed in serrated cases to improve the predictions.

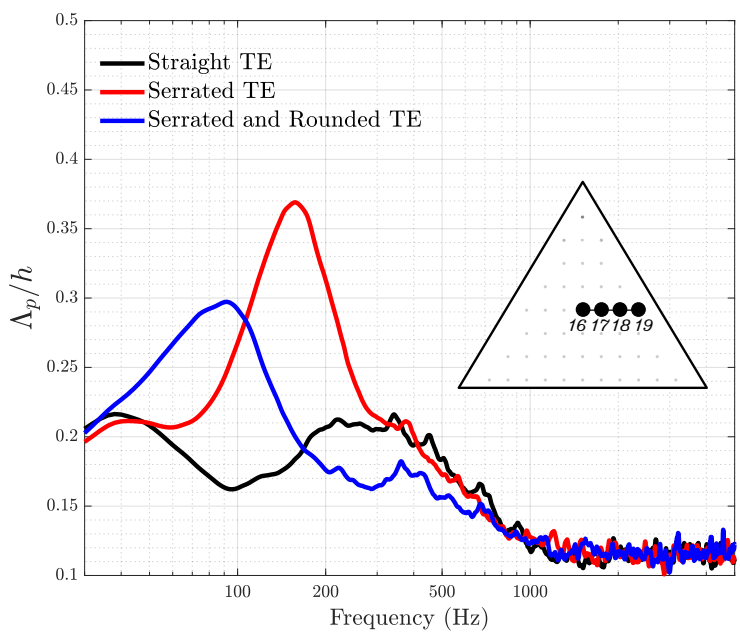

Figure 8 Span-wise length scales Λ_p based on the wall surface pressure measurement along the span at $x'/h = 60$.

3.2.2. Stream-wise coherence

Stream-wise coherence measured between the microphones are calculated using Equation3. Figure 9 presents the results of stream-wise coherence between reference microphone, shown by the marker "x", and upstream microphones at non-dimensional span-wise distances of $z/h = 0, 0.09, 0.18$ and $z/h = 0.26$. These locations are shown on the very left column of the figure. The microphones, which were used to calculate coherence with respect to reference microphone, are colour-coded. The same colour-code is also implemented in the graphs to ease the interpretation. The three columns from left to right represent the STE, SER and SER-R cases.

Considering the straight trailing edge case, STR, the trend of the stream-wise coherence does not change between the span-wise measurement locations ($z/h = 0$ to $z/h = 0.26$). A broadband hump occurs between $100Hz < f < 1200Hz$. Specifically, the coherence magnitude and frequency range is quite similar between coherence functions of mic3-mic6 at $z/h = 0$, mic4-mic7 $z/h = 0.09$, mic12-mic18 at $z/h = 0.18$ and mic19-mic26 at $z/h = 0.26$. This observation may indicate that the flow is well developed and the structures on the straight trailing edge do not change in the span-wise and stream-wise directions.

In contrast, the coherence behaviour dramatically changes with the introduction of serrations. On the symmetry line, $z/h = 0$, a very high magnitude broadband peak is present around $f = 200Hz$ between mic1 and mic3. Moreover, this peak exists for the coherence functions between the reference microphone "x" and upstream microphones until microphone 23. The broadband hump observed in STR still exists, but in lower magnitude. At $z/h = 0.09$, a similar trend with $z/h = 0$ is observed. Moving towards the serration edge profile, the magnitude of the peak at $f = 200Hz$ diminishes and a combined double hump occurs. This observation may be interpreted as follows: The strong turbulent structures are generated on the serration edge between microphone 4 ($x'/h = 0.27 \; and \; z/h = 0.09$) and microphone 12 ($x'/h = 0.49 \; and \; z/h = 0.18$) and develop towards downstream. Since these structures are not yet generated at upstream of microphone 12, the sensed effect is minimum. These results are well in-line with [21], where the vortical structures were claimed to be generated at around $x'/h = 0.5$, on the edge of the serrations. This also validates the initial assumption of applicability of the results of this study to normal sized serrations and the flow structures generated on them.

For the rounded-serrated case, SER-R, a similar double hump behaviour is observed. However, the magnitude of the peak is lower compared to the SER case and the peak frequency is at around $f = 150Hz$. An interesting result considering the measurement location $z/h = 0.27$ is the coherence magnitudes are lower than to that of STR. This unexpected result may be due to the rounded edges and requires further investigation.

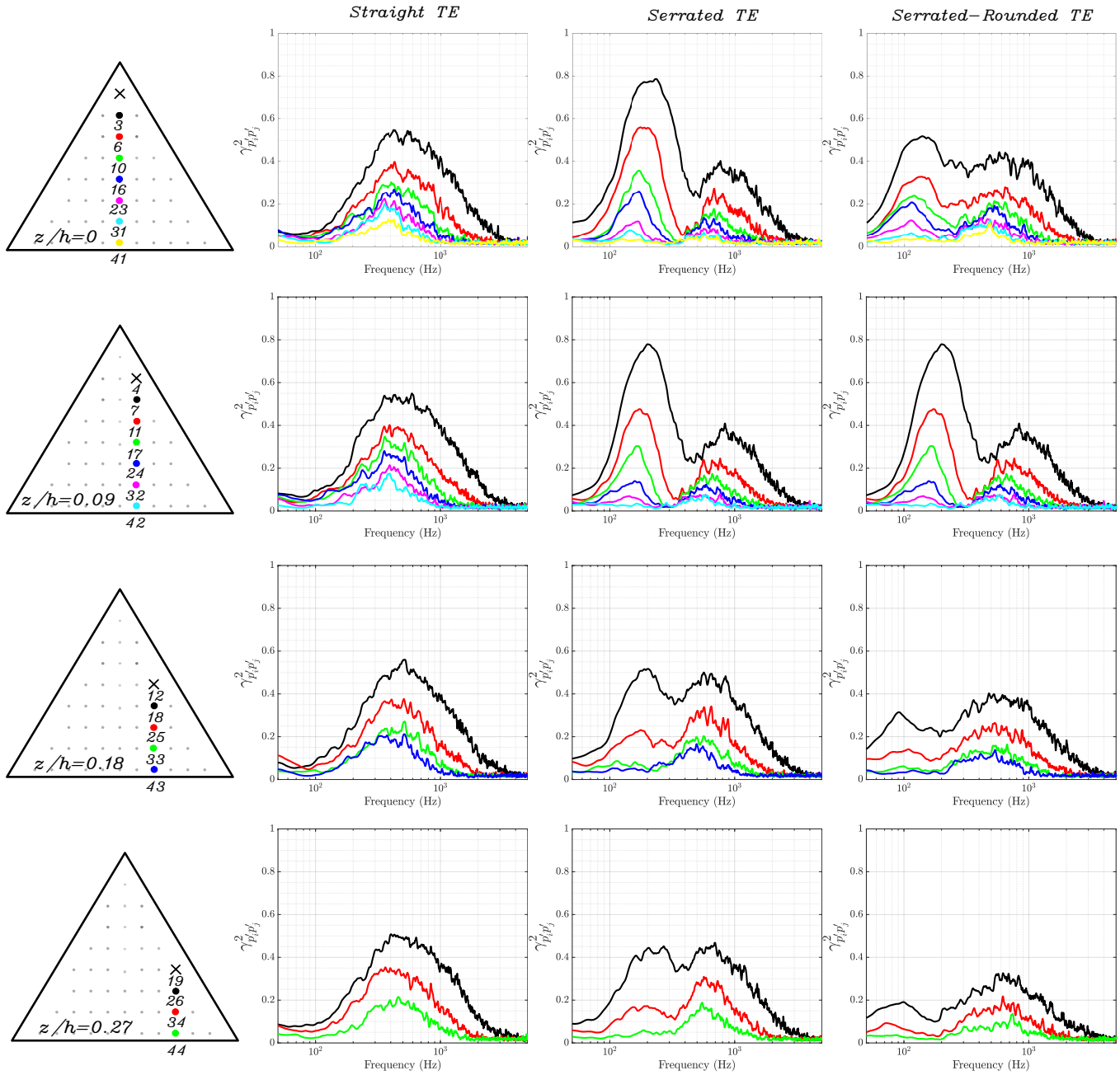

Figure 9 Comparison of stream-wise $\gamma^2_{p'_i p'_j}$ among STR, SER and SER-R span-wise stations $z/h = 0, 0.09, 0.18$ and $z/h = 0.26$ from top to bottom.

3.2.3. Temporal Correlation Analysis

To better understand the flow behaviour and assess the size of the turbulent structures, auto-correlation of the measured wall pressure is calculated using

$$R_{p_i'p_j'}(\tau) = \frac{\overline{p_i'(x_i, t+\tau)p_i'(x_i, t)}}{p'^2_{x_{i_{rms}}}}, \tag{5}$$

where p_i' is the wall pressure signal from microphones located at x_i, $p'^2_{x_{i_{rms}}}$ is the root-mean-square of the pressure fluctuation p_i' and τ represents the time delay between the signals. Two figures, consisting of four graphs, are presented to aid a more extensive evaluation flow structures on serrations. Figure 10 includes the results for microphones 1, 3, 6 and 10 located at $x'/h = 0.16, 0.27, 0.38$ and $x'/h = 0.49$ respectively. Figure 11 is constructed to show the evolution of the structures on the serration edge profile for microphones 1,4,7 and 12 which are located at the same stream-wise distances as those shown in Figure 10. The auto-correlations are plotted against the non-dimensional time $\tau U/h$.

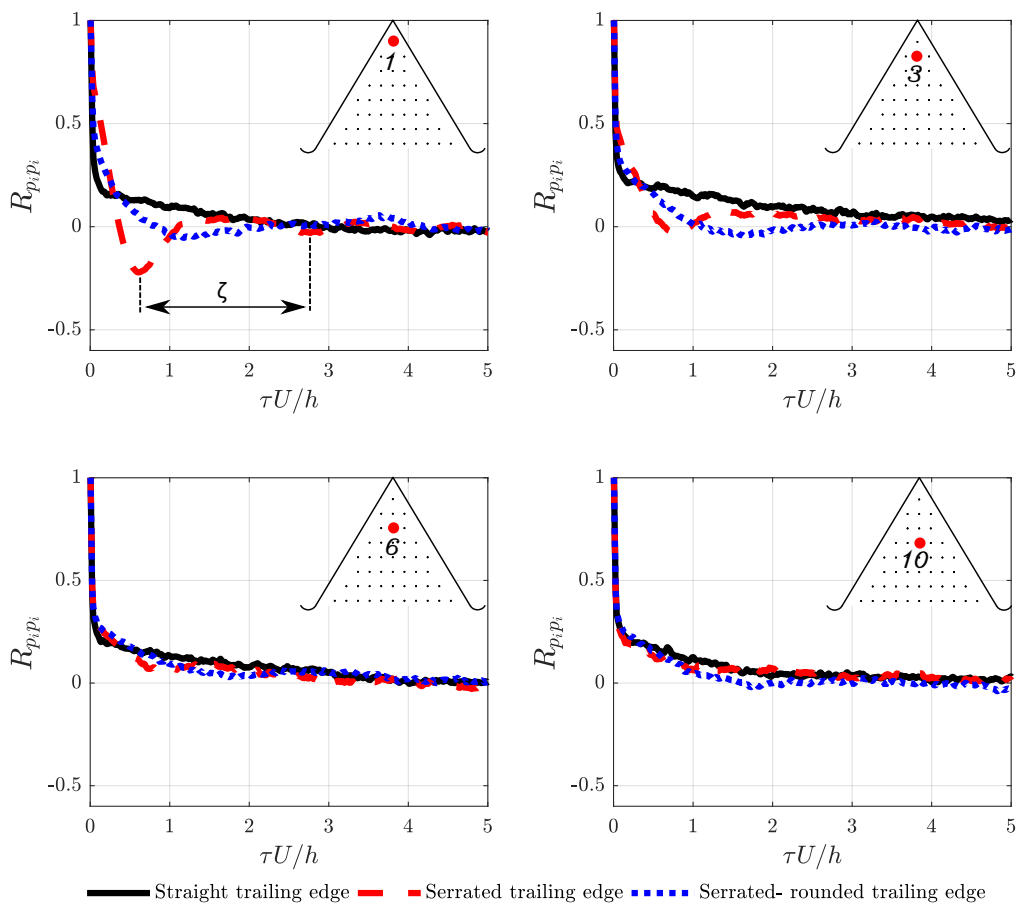

Figure 10 Autocorrelation of wall pressure fluctuations as a function of $\tau U/h$ for microphones 1,3,6 and 10 (stream-wise).

Considering the auto-correlation result for microphone 1 at $x'/h = 0.16$ in Figure 11, the STR case, shows a very fast decay at around $\tau U/h = 0$ and then slowly converges to a zero value, which is a

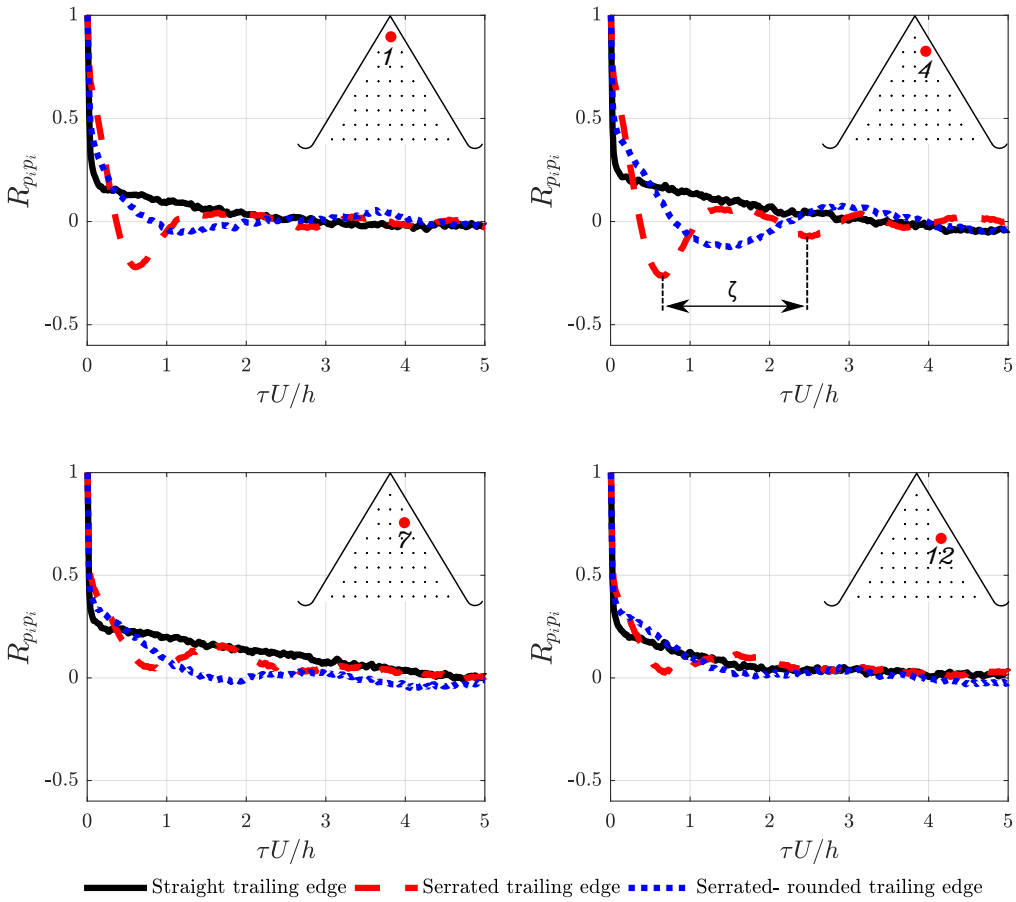

Figure 11 Autocorrelation of wall pressure fluctuations as a function of $\tau U/h$ for microphones 1,4,7 and 10 (edge-wise).

typical boundary layer auto-correlation profile. The fast decay is due to very fine scale structures in the turbulent boundary layer. The trailing edge serration, however, imposes a completely different behaviour. The slower decay and the large negative cusp are an indicator of the larger scale vortical motions in the boundary layer [22]. The oscillation periodicity ζ is an indicator of a quasi-periodic stream-wise vortical structure organization. The periodicity $\zeta = 2.13$ refers to an hydrodynamic event at $f = 153Hz$. For SER-R case the quasi-periodicity is hardly pronounced. At microphone location 3, although this behaviour still exist, it appears as if it is damped. Moving further upstream all cases collapse into a similar trend.

In Figure 11 the effect that the serration creates is more prominent and the oscillatory behaviour is observable over the entire upstream stations. At microphone location 4, the oscillation periodicity is similar, however the negative cusp is even deeper for both SER and SER-R case. At microphone locations 7 and 12, the quasi-periodicity is still observable but with lower correlation magnitude. This is a further validation of the importance of the edge profiles on generated turbulent structures.

4. Conclusion

The present study investigates the effect of large serrations on trailing-edge noise generated through the flow past a flat plate. Emphases are placed on the detailed mapping and analyses of near-wall pressure fluctuations, by means of steady and unsteady pressure measurements.The experiments are conducted in an open-jet anechoic wind tunnel at serration length h based $Re = 1.8x10^5$ for two different configuration for serrations. The power spectral density of the measured pressure (ϕ_{pp}) and fluctuating pressure distribution suggest that an elevated energy content exists for the serrated cases, which possibly contributes to the broadband hump observed along the surface ϕ_{pp} at relatively low frequencies between $50Hz < f < 600Hz$. Results from stream-wise and span-wise coherence analyses further corroborates these observations and indicate that a noticeable difference between the peak frequencies of the hump between straight ($200Hz$) and rounded serrations ($150Hz$). Last but not least, temporal auto-correlation on the surface microphones points to the presence of large scale vortical motions along the serrations, as compared to that of a developed profile for conventional straight trailing-edge flat plate. The present results affirm the notion that serrations play an important role in modifying the generation of trailing-edge noise and their different length scales should be accounted for when to predict the associated far-field noises.

Acknowledgments

The authors would like to thank Dr. Syamir Alihan Showkat Ali and Mr. Jonathon Luke Bowen for their valuable contributions.

References

[1] T.F. Brooks, D.S. Pope, and M.A. Marcolini. *Airfoil self-noise and prediction*. Tech. rep. National Aeronautics of Space Administration, Office of Management, 1989.

[2] M. Herr and W. Dobrzynski. “Experimental Investigations in Low-Noise Trailing Edge Design”. In: *AIAA Journal* 43.6 (2013), pp. 1167–1175.

[3] B. Lyu, M. Azarpeyvand, and S. Sinayoko. “Prediction of noise from serrated trailing edges”. In: *Journal of Fluid Mechanics* 793 (2016), pp. 556–588.

[4] X. Liu et al. “Aerodynamic Performance and Wake Development of Airfoils with Serrated Trailing-Edges”. In: *AIAA Journal* 55.11 (2017), pp. 3669–3680.

[5] S.A. Showkat Ali, M. Azarpeyvand, and C.R. Ilário da Silva. “Trailing-edge flow and noise control using porous treatments”. In: *Journal of Fluid Mechanics* 850 (2018), pp. 83–119.

[6] S.A. Showkat Ali et al. “Boundary layer flow interaction with a permeable wall”. In: *Physics of Fluids* 30.8 (2018), p. 085111.

[7] A. Wolf et al. “Trailing edge noise reduction of wind turbine blades by active flow control”. In: *Wind Energy* 18.5 (2015), pp. 909–923.

[8] M. Szoke and M. Azarpeyvand. “Active Flow Control Methods for the Reduction of Trailing Edge Noise”. In: Proceedings of the 23rd AIAA/CEAS Aeroacoustics Conference, Denver, CO. AIAA 2017-3004.

[9] M. Szőke, D. Fiscaletti, and M. Azarpeyvand. “Effect of inclined transverse jets on trailing-edge noise generation”. In: *Physics of Fluids* 30.8 (2018), p. 085110.

[10] I. Ayumur, N. Chiho, and A. Masahito. “Suppression of Tonal Trailing-Edge Noise From an Airfoil Using a Plasma Actuator”. In: *AIAA Journal* 51.7 (2013), pp. 1695–1702.

[11] S. Oerlemans et al. “Reduction of Wind Turbine Noise Using Optimized Airfoils and Trailing-Edge Serrations”. In: *AIAA Journal* 47.6 (2013), pp. 1470–1481.

[12] M.S. Howe. “Noise produced by a sawtooth trailing edge”. In: *The Journal of the Acoustical Society of America* 90.1 (1991), pp. 482–487.

[13] B. Lyu and M. Azarpeyvand. “On the noise prediction for serrated leading edges”. In: *Journal of Fluid Mechanics* 826 (2017), pp. 205–234.

[14] M. Azarpeyvand and Joseph P.F. Gruber M. “An analytical investigation of trailing edge noise reduction using novel serrations”. In: Proceedings of 19th AIAA/CEAS Aeroacoustics Conference, Berlin, Germany. 2013.

[15] D. Ragni et al. “Measurements of near-wall pressure fluctuations for trailing-edge serrations and slits”. In: *Experiments in Fluids* 60.1 (Nov. 2018), p. 6.

[16] L.E. Jones and R.D. Sandberg. “Acoustic and hydrodynamic analysis of the flow around an aerofoil with trailing-edge serrations”. In: *Journal of Fluid Mechanics* 706 (2012), pp. 295–322.

[17] F. Avallone, W.C.P. van der Velden, and D. Ragni. “Benefits of curved serrations on broadband trailing-edge noise reduction”. In: *Journal of Sound and Vibration* 400 (2017), pp. 167–177.

[18] R.D. Sandberg and L.E. Jones. “Direct numerical simulations of low Reynolds number flow over airfoils with trailing-edge serrations”. In: *Journal of Sound and Vibration* 330.16 (2011), pp. 3818–3831.

[19] M. Gruber and Joseph P.F. Azarpeyvand M. “Airfoil trailing edge noise reduction by the introduction of sawtooth and slitted trailing edge geometries”. In: Proceedings of 20th International Congress on Acoustics, ICA 2010, Sydney, Australia. 2010.

[20] F. Avallone, S. Pröbsting, and D. Ragni. “Three-dimensional flow field over a trailing-edge serration and implications on broadband noise”. In: *Physics of Fluids* 28.11 (2016), p. 117101.

[21] T.P. Chong and A. Vathylakis. “On the aeroacoustic and flow structures developed on a flat plate with a serrated sawtooth trailing edge”. In: *Journal of Sound and Vibration* 354 (2015), pp. 65–90.

[22] C.K.W. Tam et al. “The sources of jet noise: experimental evidence”. In: *Journal of Fluid Mechanics* (2008), pp. 253–292.

[23] Y.D. Mayer et al. “Design of an Aeroacoustic Wind Tunnel Facility at the University of Bristol”. In: Proceedings of the 24th AIAA/CEAS Aeroacoustics Conference , Atlanta, GA. AIAA 2018-3138.